Journal of Materials Science and Chemical Engineering, 2025, 13(2), 1-22
https://www.scirp.org/journal/msce
ISSN Online: 2327-6053
ISSN Print: 2327-6045

Physical, Thermal and Mechanical Characterization of Epoxy/Rafia Vinifera Woven Composite Materials: Application to the Comfort of Boats in Tropical Areas

Alfred Kendem Djoumessi[1,2,3*], Nicodème Rodrigue Sikame Tagne[1,2,3], Elvis Mbou Tiaya[3], Augustine Demze Nitidem[3,4], François Ngapgue[1,2], Ebenezer Njeugna[3,4]

[1]Research Unit in Mechanics and Modeling of Physical Systems (UR2MSP), Faculty of Sciences, University of Dschang, Dschang, Cameroon
[2]Industrial Environment and Systems Engineering Research Unit (URISIE), IUT/FV Bandjoun, University of Dschang, Bandjoun, Cameroon
[3]Laboratory of Mechanics and Adapted Materials (LAMMA), ENSET, University of Douala, Douala, Cameroon
[4]Mechanics Laboratory, University of Douala, Douala, Cameroon
Email: *kendjoums@gmail.com

How to cite this paper: Djoumessi, A.K., Tagne, N.R.S., Tiaya, E.M., Nitidem, A.D., Ngapgue, F. and Njeugna, E. (2025) Physical, Thermal and Mechanical Characterization of Epoxy/Rafia Vinifera Woven Composite Materials: Application to the Comfort of Boats in Tropical Areas. *Journal of Materials Science and Chemical Engineering*, **13**, 1-22.
https://doi.org/10.4236/msce.2025.132001

Received: December 28, 2024
Accepted: February 15, 2025
Published: February 18, 2025

Abstract

The mechanical, physical and thermal characterization of a composite made from woven raffia fiber vinifiera molded in epoxy resin intended for shipbuilding shows that the density (0.5 g/cm^3 with a relative error of 0.05 g/cm^3) of the composite produced is lower than that of wood used in this field. The material has low porosity (9.8%) and is less absorbent (12.61%) than wood. The result of the thermal conductivity test by the hot plane method shows that this composite can contribute to the internal thermal insulation (an example of thermal conductivity is 0.32W/m.K) of floating boats. The mechanical tests of compression (young modulus is 22.86 GPa), resilience (1.238 J/Cm^2) and hardness (233.04 BH30-2.5/187.5-15s) show that this composite is much harder and more absorbent than many wood and bio-composite materials used in the construction of pleasure boats. The abrasion test (0.005349) shows that this composite could well resist friction with the beach.

Keywords

Density, Thermal, Resilience, Hardness, Abrasion, Raffia/Epoxy Composite

1. Introduction

The need for comfort and weight reduction in cars, planes and boats leads experts

in these different fields to look for the most suitable material to fulfill the desired function. In the field of shipbuilding, the lightness of the material allows to reduce fuel consumption [1] and contributes to improving thermal comfort. However, the material must be hard and rigid enough to withstand the hazards of the sea and the navigation environment. In shipbuilding, these problems arise more acutely, since the amount of fuel consumed by the boats is influenced by its weight. This weight depends on the density of the material used [2]. For safety reasons, knowledge of the behavior of the material under compression, impact (resilience and hardness) and abrasion is necessary. The concern for thermal comfort inside the boats is added to the problems related to the weight to be moved. In addition to the mass to be moved, shipbuilding in sub-Saharan Africa is still faced with the problem of interior comfort. The adequacy between the comfort felt inside the boat and the specific weight is the primary goal of bio composites developed for the implementation of floating boats. For this, research has been carried out to develop bio composites to implement pleasure boats, for example, the bio composite based on basalt fiber and flax mixed with epoxy to manufacture the artifact [3]. The impact behavior of fiber-reinforced composites is the concern of several researchers at present. This is particularly the case for composite reinforced with hemp, carbon and their hybrid fibers; this study shows that the hemp-reinforced material absorbs shocks better. The results obtained on the study of the penetration resistance of marine composites show that low-speed impact loads, even with low impact energy, can cause serious damage and initiate leaks in composite hulls [4]. Although these analyses aim to understand the impact reaction of various fibrous materials, the study of the impact of bio composites reinforced with plant fibers used in shipbuilding remains to be supported. Similarly, the study of friction between the hull and the beach sand remains to be specified in order to evaluate the removal of material in contact with the beach. The objective of this work is to determine the resilience, hardness and abrasion coefficient of the raffia fiber/epoxy resin composite, in order to evaluate its ability to be used for the construction of small boat hulls. The effect of seawater over time is the deterioration of bio composite, water absorption reaches the peak after one month [5]. Research shows that bio composite with woven reinforcement structure has good thermal stability [6], also that their hybridization stabilizes their thermal and flammability properties [7], as well as the influence of fiber diameter for morphology analysis [8] and fiber cooling performance [9]. In addition, woven reinforcements have already shown their thermal comfort ability in the textile field [10]. In addition, the use of epoxy shows that it is a good thermal insulator. But the wear rate of the composite made by epoxy increases as well as the sliding frequency or temperature [11]. The study of the thermal cycle in woven laminated composites shows that the temperature can cause delamination by interlinear fracture [12]. The raffia fiber has pigs on its surface, this can allow it to be used as a thermal insulator [13]. The determination of the mechanical properties of the bio composite (made by woven raffia vinifera fibers and epoxy resin) was done by evaluating

the breaking force and the two weaving directions (weft and warp) [14]. The objective of this work is to develop a bio composite based on woven raffia vinifera fiber that can be used to build floating boats; then to determine its behavior to impact, abrasion, physical and thermal of the woven bio composite Raphia vinifera/epoxy. This work begins with the manufacture of the composite. Then by the characterization of the physical, thermal and mechanization behaviors of the bio composite. The results are then discussed and compared with those of previous works.

2. Materials and Methodology

2.1. Composite Elaboration

The detailed process of bio composite implementation is described in **Figure 1**. The material was produced by the contact molding process. This type of process keeps the pigs on the surface of the fiber. The average Young's modulus of the raffia vinifera fiber used is 4.4 GPa [15]. The Young's modulus of the epoxy resin used is 3.1 GPa in tension. The mass fraction of the woven fiber structure is 25% of the total mass of the composite. The epoxy resin was mixed with a hardener at 40% volume fraction. In accordance with ISO 8302:1991, the bio-composite sample plates were cut to dimensions ($10*10*1$ cm^3) and placed in molds. The resin was then cast. The process diagram is shown in **Figure 1**.

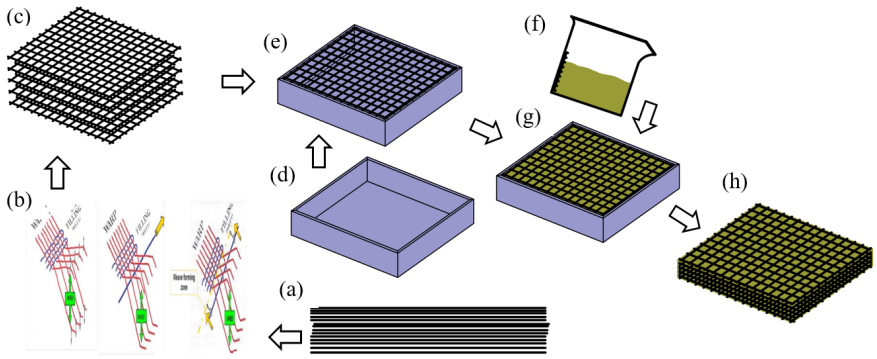

Figure 1. Composite development process; (a) Raphia vinifiera fibers, (b) fiber weaving process, (c) woven reinforcement structure, (d) mold, (e) molding of the woven reinforcement structure, (f) epoxy resin, (g) shaping of the composite, (h) biocomposite obtained.

2.2. Physical Characterization

The main equipment used for physical characterization is a digital milligram balance (0.001 g), a milliliter beaker (0.001 l), a millimeter caliper (0.001 m), distilled water and containers.

2.2.1. Apparent and Real Density of the Composite

There are two approaches to determining the density of the biocomposite; that by direct weighing, dimension measurement then calculation of volume (apparent mass) [16] according to the ASTMD 792 standard. The expression of the apparent mass is given by Equation (1).

$$\rho_{ap} = \frac{m}{V_{th}} \tag{1}$$

m: mass of the composite (kg); V_{th} : theoretical volume of the composite (m^3).

As for the actual density (ρ_{real}), it is found by direct weighing of mass, then embedding in paraffin then immersion in distilled water contained in a graduated volume (beaker), the actual density is given by Equation (2).

$$\rho_{real} = \frac{m_c}{V_{en} - \frac{m_{en} - m_c}{\rho_{pa}}} \tag{2}$$

with m_c : mass of the composite (kg), V_{en} : volume of the coated composite (m3), m_{en} : mass of the coated composite (kg), ρ_{pa} : density of the paraffin (kg/m 3). Using the actual and volumetric density, the porosity of the composite is deduced by Equation (3).

$$P = \frac{\rho_{real} - \rho_{ap}}{\rho_{real}} * 100 \tag{3}$$

where: P is the porosity of the woven composite material.

2.2.2. Water Absorption Rate of the Composite

It is noted (τ) and is done according to the ISO 62:2008 standard. The test consists of weighing the samples (ten), then immersing them in distilled water and carrying out successive weighings until saturation. The balance used is calibrated to the milligram. The expression for the absorption rate from [14] is given by Equation (4).

$$\tau = \frac{m_f - m_i}{m_i} * 100 \tag{4}$$

where M_f : saturation mass (kg) and M_i : initial mass (kg).

2.3. Thermal Characterization

The thermal properties of the composite material are determined by the asymmetric hot plane method with an insulated back face. The principle is to send a constant flow of heat into a heating element using a stabilized power supply whose power input is 220 V and the output varies from 0 to 30 V. The heating element with thermocouple K is in contact with the face of the sample and the temperature on this face of the sample is recorded by an 8-channel Picolog to which a temperature sensor is connected [17]. In this particular case, the temperature range was between the ambient temperature, which is considered as the initial temperature (32˚C), and the maximum temperature obtained in the case of this test, which is of the order of 50˚C. The Picolog recorder is connected to the computer which made it possible to interface the recording. This method is used by several authors such as [18]. The measurement uncertainties of the equipment are of the order of a thousandth. The unidirectional heat transfer model is given by Equation (5). Different from the rotating heat flow [19].

$$\begin{pmatrix}\theta_c\\ \Phi_{01}\end{pmatrix}=\begin{pmatrix}1 & 0\\ C_{hP} & 1\end{pmatrix}\begin{pmatrix}1 & SR_{chs}\\ 0 & 1\end{pmatrix}\begin{pmatrix}A_s & B_s\\ C_s & D_s\end{pmatrix}\begin{pmatrix}1 & S_sR_{csi}\\ 0 & 1\end{pmatrix}\begin{pmatrix}A_i & B_i\\ C_i & D_i\end{pmatrix}\begin{pmatrix}0\\ \Phi_1\end{pmatrix}$$
$$\begin{pmatrix}\mathbf{A_s} & \mathbf{B_s}\\ \mathbf{C_s} & \mathbf{D_s}\end{pmatrix}\begin{pmatrix}0\\ \mathbf{\Phi}_1\end{pmatrix} \quad (5)$$

The following working conditions are permitted:

The hot flow propagates in one direction only;

The work materials are at ambient temperature;

There is no heat loss during the experiment;

The contact between the heating element and the insulation is resistance-free;

Polystyrene blocks are considered to be semi-infinite media.

The heat received by the sample from the heat source is given by Equation (6) [20].

$$\begin{pmatrix}\theta_c\\ \Phi_{01}\end{pmatrix}=\begin{pmatrix}1 & 0\\ \rho_h c_h e_h p & 1\end{pmatrix}\begin{pmatrix}1 & SR_{chs}\\ 0 & 1\end{pmatrix}\begin{pmatrix}\theta_1\\ E\sqrt{p}\theta_1\end{pmatrix} \quad (6)$$

Equation (7) represents the heat flux received by the polystyrene block (Φ_{02}) from the element.

$$\begin{pmatrix}\theta_c\\ \Phi_{02}\end{pmatrix}=\begin{pmatrix}1 & SR_{chi}\\ 0 & 1\end{pmatrix}\begin{pmatrix}\theta_2\\ E_i\sqrt{p}\theta_2\end{pmatrix} \quad (7)$$

With E and E_i respectively the thermal efficiencies of the sample and the insulator. The unit of thermal effusivity is $\left(J.m^{-2}.K^{-1}s^{-1/2}\right)$. Combining Equations (6) and (7) gives Equation (8) [21].

$$\theta_c(z,p)=\frac{\phi_0}{p}\frac{S}{\dfrac{C_hSp+(1+C_hpR_{chs}S)ES\sqrt{p}}{1+R_{chs}SE\sqrt{p}}+\dfrac{E_iS\sqrt{p}}{1+R_{chi}SE_1\sqrt{p}}} \quad (8)$$

Equation (9) represents the inverse transform of this function for sufficiently long times ($t \to +\infty$) i.e. in the Laplace domain+ when ($p \to 0$).

$$\Delta T(0,t\to+\infty)=\phi_0 S\left(\frac{E^2R_{chs}+E_i^2R_{chi}}{(E+E_i)^2}-\frac{C_h}{S(E+E_i)^2}\right)+\frac{2\phi_0}{(E+E_i)\sqrt{\pi}}\sqrt{t} \quad (9)$$

The square root of time characterizes the heat variation within the source that generates it. The thermal effusivity of the sample can be pre-estimated from the one-dimensional model by calculating the slope a of the experimental curve between two times t and $t+dt$. It is presented in Equation (10).

$$\Delta T(0,t)=f\left(\sqrt{t}\right) \quad (10)$$

In this way, over a time interval the curve is assimilated to a straight line. From then on, the calculation is carried out on the linear third of the curve. Equation (11) presents the slope of the straight line.

$$\alpha=\frac{T(t+dt)-T(t)}{\sqrt{t+dt}-\sqrt{t}} \quad (11)$$

By identification with Equation (9), the slope is given by Equation (12)

$$\alpha = \frac{2\phi_0}{(E + E_i)\sqrt{\pi}} \tag{12}$$

The thermal effusivity of the sample can be deduced from Equation (12) by the Equation (13)

$$E = \frac{2\phi_0}{\alpha\sqrt{\pi}} - E_i \tag{13}$$

Over an infinitely small-time interval, the heat transfer δq crossing a probe allows to appreciate the thermal density, as noted in Equation (14).

$$\phi_0 = \frac{\delta q}{dt} \tag{14}$$

Equation (15) shows the distribution that can be made of the heat transfer in case of an increase in temperature due to the flow.

$$\phi_0 dt = q_e + q_i + q_s \tag{15}$$

Here q_e is the amount of heat passing through the sample; q_i is the amount of heat passing through the insulating block and q_s is the amount of heat passing through the probe. Joule's law gives the amount of heat according to mass, specific heat and temperature in Equation (16).

$$\delta q = mC_p dT \tag{16}$$

The heat flux dissipated by the probe also causes a rise in the temperature of the polystyrene block (insulation) and the material. Taking into account the definitions of Equations (15) and (16) we have Equation (17).

$$\phi_0 = \left(\rho C_p e + \rho_i C_{pi} e_i + \rho_s C_{ps} e_s\right)\frac{dT}{dt} \tag{17}$$

By plotting the curve $\Delta T = f(t)$ and exploiting the linear part of the curve, the slope of the curve is defined by the relation Equation (18).

$$\gamma = \frac{dT}{dt} = \frac{T(t + dt) - T(t)}{dt} \tag{18}$$

Exploiting Equation (17) and the relation allows us to obtain the volumetric heat by Equation (19).

$$\rho C_p = \frac{1}{e}\left(\frac{\phi_0}{\gamma} - (\rho C_p e)_i - (\rho C_p e)_s\right) \tag{19}$$

Inversion by the De Hoog algorithm will allow to find the theoretical temperature of the complete model. Figure 2 shows the principle diagram of the heat transfer.

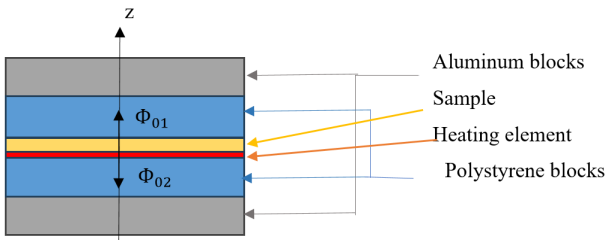

Figure 2. Schematic of heat transfer.

Thanks to the Levenberg-Marquardt algorithm coded in MATLAB, we have an interval $[t_0; t_{max}]$ on which the residual curve is centered around 0˚C, the values of E and ρCp (taking as initial value the pre-estimated values) which minimize the sum of the squares of the errors between the modeled value of the observed temperature $T_{mod}(t)$ and the value obtained experimentally $T_{exp}(t)$.

2.4. Mechanical Characterization

All the experimental tests have been carried out with the Douala ambient temperature (32˚C) and 68% relative humidity

2.4.1. Compression Test

The compression test is carried out according to the NBN B15-220 standard [7].

Figure 3 gives an image of the testing machine. The measuring comparators have an uncertainty of one millimeter. The test was carried out on 15 samples.

Figure 3. Compression testing machine.

The test is performed using two springs; the first gives the value of the compression of the ring Δx of stiffness (K = 121740 N/mm) and the second the compression of the sample (Δe). The graph F(Δe) is plotted to obtain the Young's modulus of the composite in compression. The force exerted on the sample is obtained using E Equation (20)

$$F = K\Delta x\,. \tag{20}$$

Subsequently, we calculate the Young's modulus in compression by Equation (21)

$$E = \frac{e\Delta F}{Ll\Delta e} \tag{21}$$

The expression ΔF/Δe is given by the slope of the curve F(Δe). Hence:

e: thickness of the sample, L: length of the sample and l: width of the sample.

The experimental curves are plotted by converting the video of the comparator values variations into an image as presented by [8].

2.4.2. Resilience Test

This test assesses the potential to withstand shocks without deteriorating or breaking. The test is carried out on a Charpy type machine (test specimen on two supports). The samples are cut to meet the requirements of ASTM E23. The test was carried out on 15 samples. The uncertainty of reading the test dial is 1 degree. Figure 4 gives the principle of Charpy test.

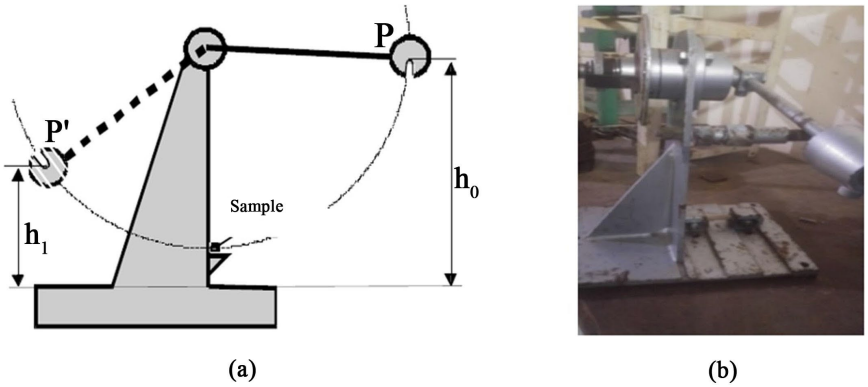

Figure 4. Charpy test; (a) test principle, (b) testing machine.

The experimental protocol consists in dropping a hammer of known mass (m) located at the end of the arm of a pendulum of length (L) rotating in a vertical plane around a horizontal axis. The pendulum is dropped from its initial position at zero speed onto a sample. Without the sample, it describes i; with the sample it describes another angle θf due to the percussion and the rupture of the sample upon contact with the mass. The resilience (K) (J/cm^2) is obtained by the ratio of the absorbed energy to the cross-section of the notched area on the sample. It is given by Equation (22):

$$K = W/S \tag{22}$$

The absorbed energy is obtained using Equation (23)

$$w = w_i - w_f = Ph_i - Ph_f = P\left(h_i - h_f\right) = mgl\left(\cos\theta_f - \cos\theta_i\right) \tag{23}$$

With l: arm length (32 cm), w_i: Potential energy of the forward pendulum (joule);

w_f: Potential energy of the pendulum after (joule), m: mass of the projectile (1 kg), hi: initial fall height, h_f: final fall height, S: section of the test piece (cm^2).

2.4.3. Hardness Test (HB)

Hardness testing may seem abstract and difficult to understand for some. Mastering the vocabulary and reading the hardness value demystifies the subject. The hardness test is defined by 3 criteria, letters and numbers. The hardness value is always placed before the test criteria. The Brinell test performed consists of applying a load for a determined time by a ball, and measuring the diameter of the imprint. The Brinell number is the result of the ratio between the applied load and the surface area of the spherical cap of the imprint. The Brinell test standard [10]:

ISO 6506 and ASTM E10 were followed to perform the test. In the specific case of this work, we used a durometer to obtain the hardness value directly by reading. Figure 5 represented the hardness test principle.

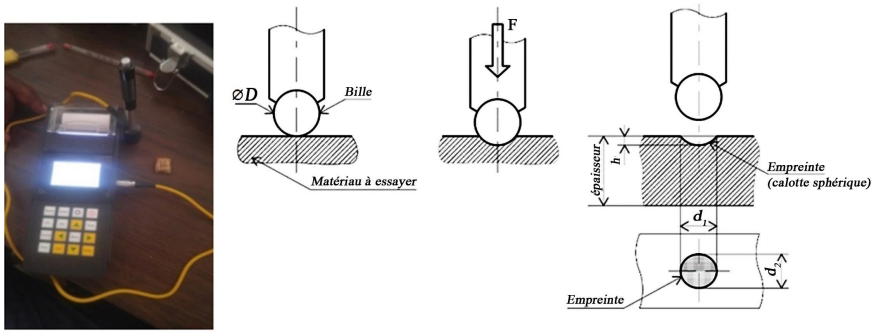

Figure 5. Durability test (a) Image of the durometer and (b) the principle of Brinell hardness.

2.4.4. Abrasion

Abrasion is used to determine the loss of material due to friction with another material. In this work, sandpaper was glued to the engine plate (6); in order to imitate the effect of the bottom of a boat rubbing on the beach. Abrasion is measured here using the tribometer opposite. **Figure 6** presents the pin disk tribometer.

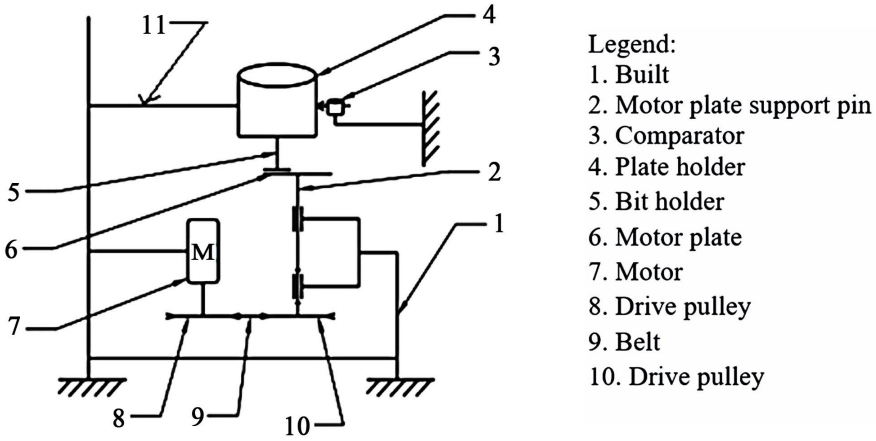

Figure 6. Pin disk tribometer [8].

The experimental protocol implemented to determine the specific wear of the material was developed by [8]. The wear is obtained by Equation (24):

$$w = \frac{1}{2\pi rn} \times \frac{1}{Fm} \times \frac{\Delta m}{\rho} \tag{24}$$

Δm: mass variation (initial mass before the test minus final mass after the test), ρ: sample density, n: number of revolutions (engine speed is 1380 rpm) during operation for 5 seconds it makes 115 revolutions or a linear speed of 43.332 m/s

(722.2 km/h or 389.1164 knots), r: the friction radius is 60 mm, Fm: The friction force due to a normal load of 55 N is given by modeling the steel bar.

Determination of the friction force involves modeling the steel bar carrying the axle, this given by Equation (25).

$$Fm = \frac{3EI}{L^3} \Delta_{\max} \tag{25}$$

The quadratic moment is given by Equation (26)

$$I = \frac{l\, e^3}{12} \tag{26}$$

Δmax: displacement given by the comparator, E: Young's modulus of steel 20500 Mpa, I: quadratic moment, L: length of the pawn arm (320 mm).

3. Results and Discussions

3.1. Physicochemical Properties

3.1.1. Density

The average density obtained from this an average value of 0.5 g/cm^3 with a relative error of 0.05 g/cm^3. As for the actual density test the porosity, it is 9.8%. The low density of the composite is 0.45 g/cm^3 with a relative error of 0.045 g/cm^3, however, the apparent density has important in the implementation of insulation materials, however this density depends on the quantities and nature of the starting materials used., the low density of this composite is due to the higher fraction of fibers which corresponds to the result of a recent publication which shows that the density decreases with the increase in fibers [22]. This composite is lighter than particle-reinforced composites such as doum and polypropylene particles [23] and many woven-reinforced composites such as flax fiber woven [2].

3.1.2. Absorption

The mixture of the highly absorbent vinified raffia fiber [24] with the hydrophobic epoxy gives a resulting absorbent biocomposite resulting composite, the same observation have been done with the random vinifera fiber epoxy [25]. The composite absorbs after 100 days a quantity of water worth 12.61% of its initial weight with a standard deviation of 1.13. This absorption rate can decrease if the implementation process is improved or changed. Compared to wood in **Table 1**, to other materials used in shipbuilding. This material has the lowest water absorption rate. In addition, this material is less absorbent than other composites made from raffia fiber. The analysis of the absorption kinetics shows the increase in water uptake by the material over time. The experimental curve of the absorption kinetics shows that the water absorption is rapid in the first days due to the high cellulose content and the pigs on the surface of the raffia fiber. This same phenomenon is observed in other works where the composite was made using epoxy resin, including [25] and [18]. This absorption behaves and the use of epoxy shows that it is a good thermal insulator typical of many composites [26]. Compared with the local shipbuilding timber shown in **Table 1**, the developed bio composite

exhibits better physical properties. The absorption behavior is depicted in Figure 7.

Figure 7. Absorption kinetics of the average sample.

Table 1. Diffusion coefficient of some wood species used in shipbuilding [27].

Drink	Mahogany	Ayous	Azobe	Doussie	Iroko	Makore	Moabi	Okoume	Sapele	Sipo
Density (g/cm^3)	0.57	0.38	1.06	0.8	0.64	0.69	0.87	0.44	0.69	0.62
Absorption rate (%)	28	29	28	19	23	28	23	40	29	30
Humidity (m^2/s) at 40˚C		2231 * 10^{-10}	2.64 * 10^{-14}		4.67 * 10^{-12}				6.45 * 10^{-12}	3.82 * 10^{-12}

3.2. Thermal Properties

One of the reasons for bio-composites in the maritime field is their contribution to thermal insulation. Figure 8 shows the result of the heat transfer test through the developed bio composite.

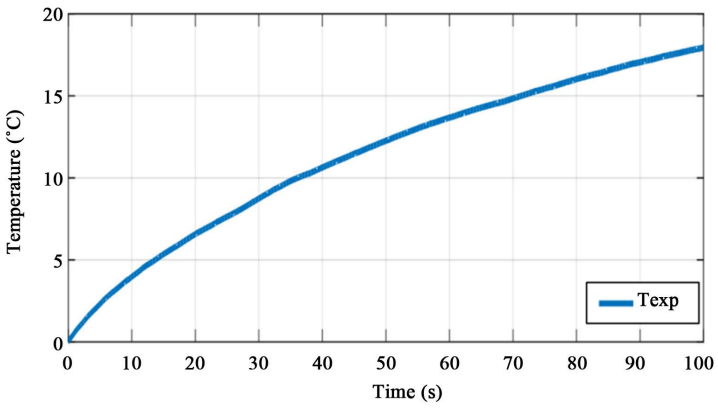

(a)

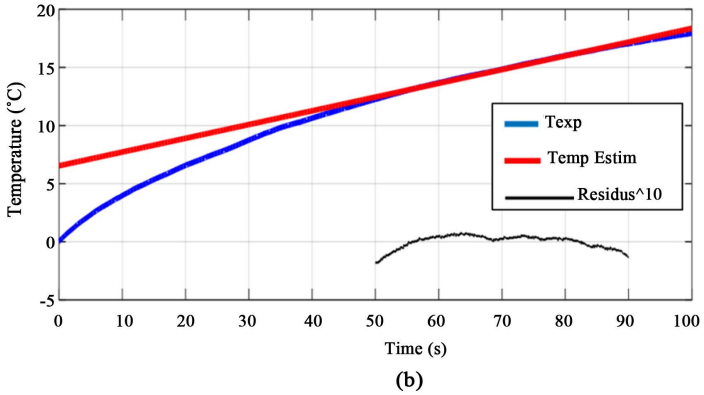

Figure 8. Heat volume curves as a function of temperature and time: (a) temperature as a function of time, (b) interpolation by estimated time.

It is observable on the curve at the interpolations equivalent to 100 seconds that the resulting temperature exchange is 18˚C, however the real time range used for the calculation is (50 to 90 seconds) in this interval the interpolation error is minimal (minimal residual). The two curves in Figure 8 show the evolution of the heat flow through the bio composite per unit of time. All the values obtained are presented in **Table 2**. The effusivity is obtained by observing the increase in temperature as a function of the square root of time; this is presented in **Figure 9**.

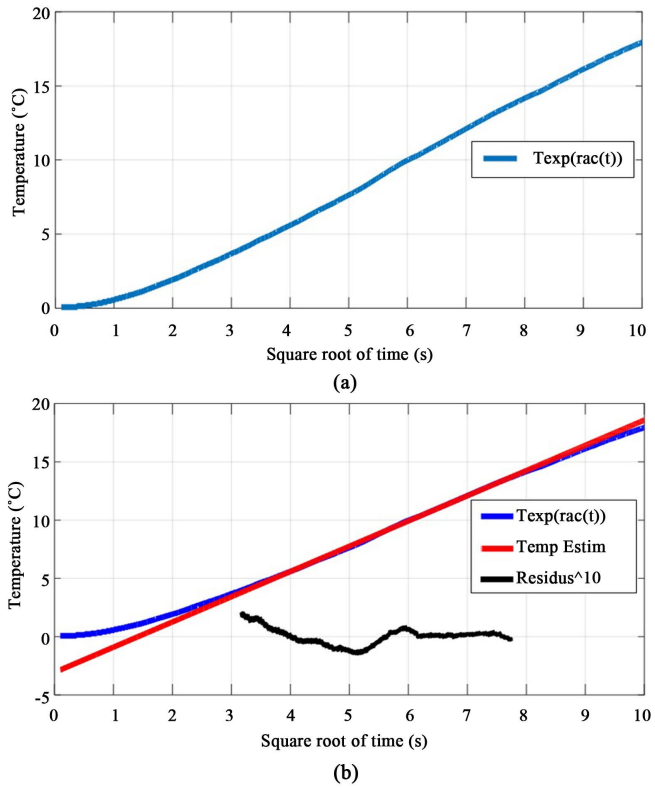

Figure 9. Temperature evolution as a function of the square root of time Thermal effusivity curves: (a) Temperature variation as a function of the square root of time, (b) interpolation as a function of the estimated time.

In the interpolation interval (place of minimum error) all thermal parameters were calculated. All values obtained are summarized in Table 2.

Table 2. Summary of heat transfer values.

	Effusivity (J/m 2 Ks 1/2)	Heat capacity (J/m^3K)	Conductivity (W/mk)	Diffusivity (m^2/s)
Example 1	229.42	183319.46	0.287	1.57E-06
Example 2	335.32	306898.59	0.37	1.19E-06
Example 3	231.7	183321.01	0.28	1.55E-06
Example 4	314.87	260846.83	0.38	1.46E-06
Example 5	331.02	216582.17	0.32	1.51E-06
Average	288.46	230193.61	0.32	1.46E-06
Standard deviation	53.41	53391.87	0.04	1.52E-07
Variance	0	0	0	0

The similarity of the values in the table to those of the work on the determination of the thermal properties of a bio composite for construction [28] shows that the bio composite developed can be used in insulation. Likewise, these values are close to those of the hybrid composite obtained from raffia particles and resin [18]. In addition, these values are very low compared to those used in high energy efficiency buildings [29]. In addition, the shapes of the curves obtained are similar to those of other works [17] and [30] which used the same process to develop their composite. In addition, this composite offers better overall thermal insulation than some tropical woods used in shipbuilding [31]. Its thermal conductivity is also lower than that of some bio-composites for a given range of humidity values [32] and [33], as presented in Table 3.

Table 3. Comparison of the composite with those in the literature.

	Absorption rate (%)	Thermal conductivity (W/m K)	Thermal effusivity (J/m² Ks 1/2)	Thermal diffusivity a * 10^{-7} (m²/s)	Thermal density (MJ/m³ K)	References
Raffia vinifera/epoxy woven composite material	12.61	0.28 - 0.36	229 - 335	11.9 - 15.7	0.18 - 0.3	Case study
Raphia vinifera (RV)	54 - 94	0.125 - 0.282	333 - 568	1.08 - 246	0.767 - 154	[18]
Raphia vinifera/Epoxy	36.12 - 71					[25]
Linen, Hemp/Epoxy	7 - 9.57					[34]
Okan Forests		0.45 - 0.6			1.5 - 2.5	[31]
Ayous Woods		0.2 - 0.25			2 - 2.4	[31]
Iroko Forests		0.19 - 0.5				[32]
Tali Forests		0.15 - 0.6				[32]
Bilinga Forests		0.15 - 0.45				[32]
Bio-composite based on wood fibers		0.057 - 0.064				[28]
Biocomposite based on rice fibers		0.056 - 0.065				[28]

Continued

Linen/Epoxy	**7.5**	[34]
Hemp/Epoxy	9.8	[34]

Generally, Table 3 shows that the global thermal conductivity of insolate material is lower than 1 (W/m K). Like other material, this raphia vinifera/epoxy woven composite material can help for boat insolation in sub-Saharan areas.

3.3. Mechanical Properties

3.3.1. Compression Test

Boat hulls are very often subjected to strong compressions due to the weight of the boat on the one hand and the water pressure on the other hand. The compression test therefore makes it possible to know the Young's modulus in compression and the limit load that the composite can support without crushing. The samples subjected to the compression test did not undergo complete destruction. However, beyond the force value of 25 KN the deformation was no longer perceptible. The average value of Young's modulus is E = 22.86 GPa with a standard deviation of 0.2. This is much higher than those obtained for the tensile and bending tests are. This test clearly shows the material's ability to work in compression. In other words, it is potential to be also used for the construction of the main structures (hulls) of boats. Table 4 clearly illustrates the possibility of using this composite in shipbuilding by comparing its compressive stress with those of the local woods used. **Figure 10** represented the curve of compression test.

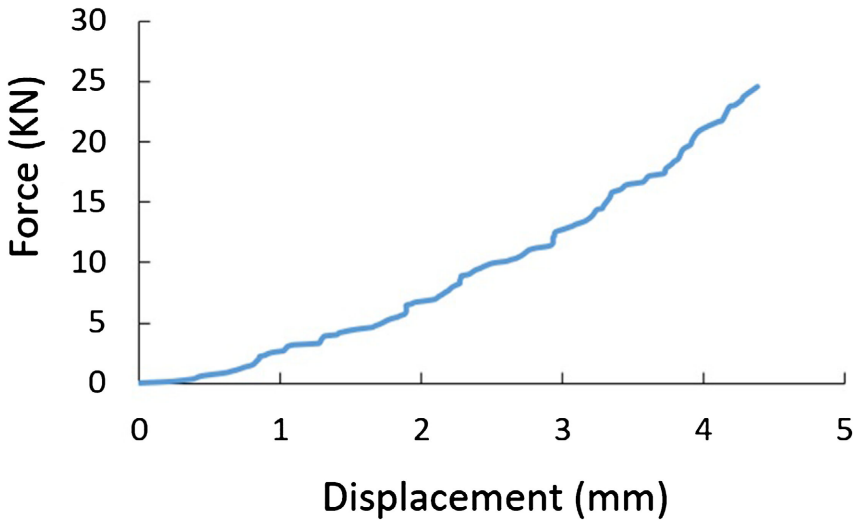

Figure 10. Compression test curve

3.3.2. Impact Test (Charpy Impact Test)

The contact due to the movement of the tide between the boats at the quay creates a shock that can lead to damage to the material used to build its hull. The resilience test was carried out experimentally on the material given in Figure 11. The value of the resilience coefficient of the different samples.

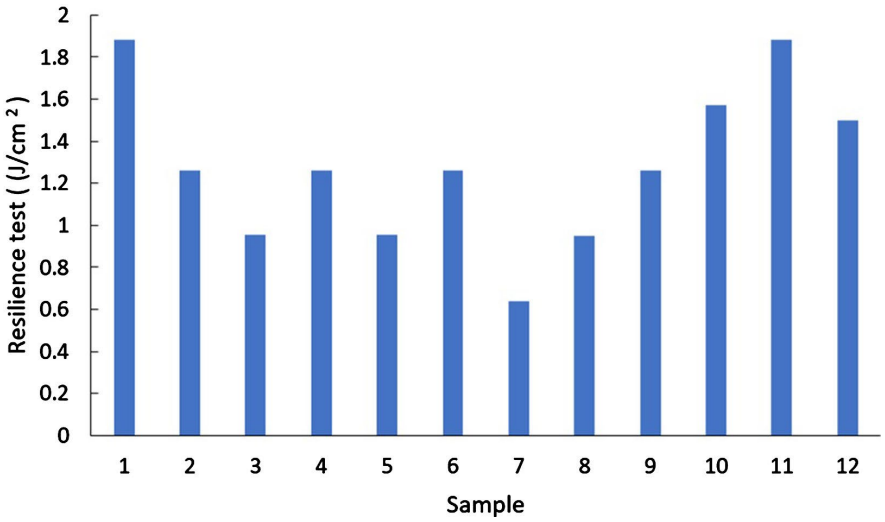

Figure 11. Result of the resilience test.

The graph in **Figure 11** gives the average value of all the points in this diagram, which is 1.238 J/Cm^2 with a standard deviation of 0.385. The value of the composite resilience is less than that of the composite with glass fiber and polymer matrix whose values are between (6.4 - 8.5 J/Cm^2) [35]. The resilience of woven reinforcement composites like other mechanical properties depends on the nature of the fibers used., for the same implementation conditions, PBO (poly(p-phenylene-2,6-benzobisoxazole), aramid, basalt, glass, and Carbon have the highest resilience value in decreasing order and natural fibers have the lowest resilience [36].

3.3.3. Hardness Test

Boat hulls collide with rocks or other boats due to maneuvering errors. The Brinell hardness test performed using the Durometer is used to assess the material's resistance to penetration and impact. **Figure 12** shows the result of all tested samples.

The average hardness value of all composite samples is given by 233.04 BH30-2.5/187.5-15s with a standard deviation of 0.25 and variance, 233.04 represents the Brinell hardness value in N/mm^2; B represents test type (Brinell); H is hardness; 15s is load application time and 30 give approximate equivalent value in Kgf of the applied test force (30 Kgf = 294.2 N).

Generally, Brinell hardness measures the depth of the imprint left by a 23 mm diameter ball, with a mass of 1 kg, thrown at 50 cm. The hardness of this material is higher than bio-sourced composites made from raffia, coconut, canarium and palm nut shell particles whose values are between (100.67 and 136.48 MPa) [37]. This shows that weaving could increase the hardness of a composite. This is the case of woven natural fibers of flax, hemp, banana, sisal, hemp, etc., all of whose mechanical properties improve compared to those of particle-reinforced composites [38].

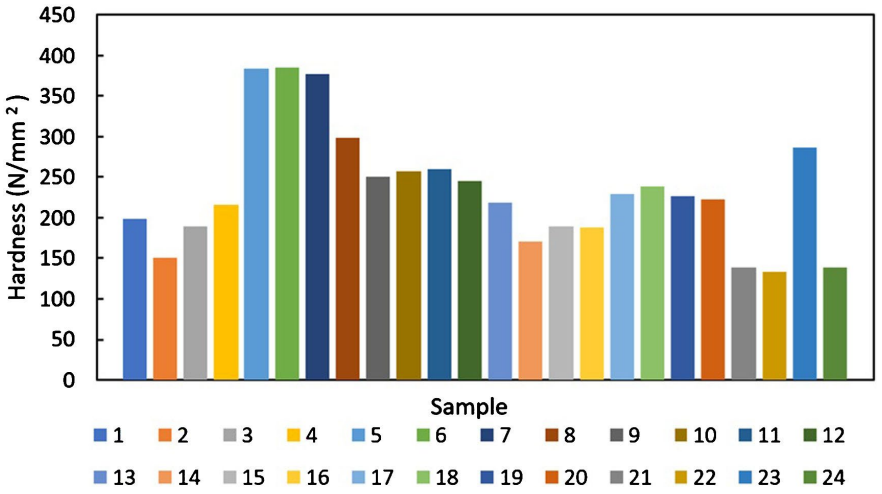

Figure 12. Hardness test result.

For wood, this test measures the resistance to punching and depending on the value obtained, the wood can be class A (soft), B (semi-hard), C (hard) and D (very hard). Compared to local woods used in shipbuilding, the developed material is admissible because its hardness is much higher than that of some of these woods. **Table 4** is an illustration of this.

Table 4. Compression, resilience, hardness and abrasion of local woods used locally in shipbuilding [14].

The woods	Compression (Breaking strength MPa)	Resilience (Nm/cm^2)	Hardness (N/mm^2)	Abrasion
Mahogany	48	3.8	33	Average
Ayous	30	3.3	24	Minimal
Azobe	96	12	145	Minimal
Doussie	74	6.8		Minimal
Iroko	57	3.8	66	Average
Kosipo	55	3.2	50	Average
Makore	58	3.3	43	Important
Moabi	74			Important
Okoume	36	2	30	Important
Padouk	70			Important
Sapele	62	5.6	45	Minimal
Sipo	55	4	45	Minimal
Works presented Woven raffia/Epoxy	62.5	2	233.04	Minimal

3.3.4. Abrasion Test

Friction between the hull and the beach generally causes material removal. The experimental setup we used to idealize this phenomenon assumes a boat rubbing the beach at a speed of 389.11 knots. **Figure 13** illustrates the material removal by abrasion test curve.

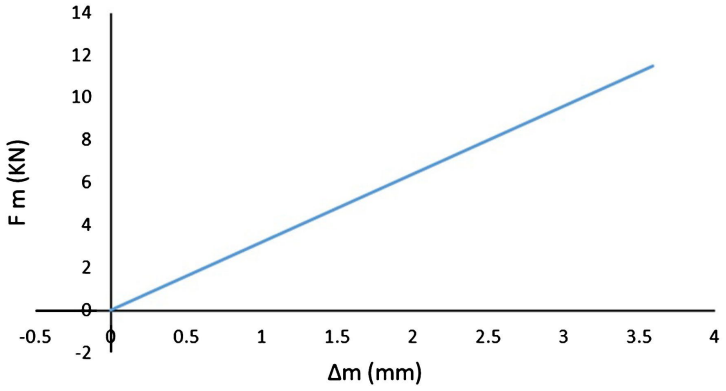

Figure 13. Abrasion test curve.

The average abrasion (wear) rate is 0.005349 and can be considered minimal. Compared to the composite based on PEEK (polyetheretherketone) matrix and reinforced with various synthetic fibers whose friction coefficient values vary between (0.6 and 1.2) [39]. In addition, for certain materials from alloys such as carbon, silicon, manganese, iron, copper, etc., the friction coefficient is between (0.1 and 0.5) [40]. It should be noted from the results in the literature that this composite cannot be used for braking applications. However, this is a satisfactory result for the desired use, because a low wear rate means minimal material tearing. This composite could be used to build hulls. Compared to the local wood used, this class is admissible. Table 4 illustrates this. In addition to having physical, thermal and mechanical properties comparable to local wood used in shipbuilding, this composite made from woven raffia fibres cast in epoxy resin is a better thermal insulator, lighter and harder than many resin-based composites, as shown in **Table 5**.

Table 5. Comparison of density, impact strength and abrasion resistance of the composite with the literature.

Composite material	Density (g/cm^3)	Absorbed impact energy (J)	Abrasion	Reference
Recycled PET fibers			0.12	[41]
Bamboo/epoxy composite for boat hull		1		[42]
Ipomoea carnea/epoxy composite	0.9		0.3	[43]
Epoxy viscose non-woven fabric	1.2	2.19	0.01	[44]
Abaca/epoxy woven composite		11		[45]
Reinforced hybrid epoxy composite		3.85		[46]
Composite jute, abaca/epoxy		15/16		[47]
Current work	0.5	2	0.005	

5. Conclusion

Coastal and river navigation is becoming increasingly important in sub-Saharan Africa for fishing, transport and tourism. In order to reduce the weight of boats and ensure their internal thermal comfort, a bio-composite based on woven raffia vinifiera fiber and epoxy resin was developed. To ensure that this composite can withstand the demands of the maritime environment and ensure thermal comfort, physical, thermal and mechanical characterizations were carried out. Measurements of real density (0.45 g/cm^3) and apparent density (0.5 g/cm^3), as well as absorption (12.61%) and porosity (9%) show that this composite is less dense and less absorbent than the wood used in local shipbuilding. Measurement of thermal conductivity by the hot plane method shows that this composite can be used as thermal insulation, so it can be used for the internal comfort of floating boats. The mechanical properties of the composite, such as its shock absorption capacity (Charpy impact test) (2 J), show that the material can withstand impacts at the dock. Similarly, the result of the abrasion test (0.005) shows that the wear of the composite in contact with the beach is minimal. All the results presented in this work show that this composite could be used for the construction of hulls of small boats.

Acknowledgements

We would like to thank the laboratories that contributed to the success of this work, in particular LAMMA for making the experimental equipment available, URISIE for constantly monitoring the progress of this work, and UR2MSP for defining this work.

Conflicts of Interest

The authors declare no conflicts of interest regarding the publication of this paper.

References

[1] Renjith, R. (2018) Literature Review on Marine Applications of Composite Materials (Review of Literature). https://doi.org/10.13140/RG.2.2.31010.73920

[2] Rubino, F., Nisticò, A., Tucci, F. and Carlone, P. (2020) Marine Application of Fiber Reinforced Composites: A Review. *Journal of Marine Science and Engineering*, **8**, Article 26. https://doi.org/10.3390/jmse8010026

[3] Fragassa, C. (2016) Effect of Natural Fibers and Bio-Resins on Mechanical Properties in Hybrid and Non-Hybrid Composites. *VIII International Conference on "Times of Polymers and Composites": From Aerospace to Nanotechnology*, Naples, 19-23 June 2016, Article 020118. https://doi.org/10.1063/1.4949693

[4] Fragassa, C. (2017) Marine Applications of Natural Fibre-Reinforced Composites: A Manufacturing Case Study. In: Pellicer, E., Nikolic, D., Sort, J., Baró, M., Zivic, F., Grujovic, N., *et al.*, Eds., *Advances in Applications of Industrial Biomaterials*, 21-47. https://doi.org/10.1007/978-3-319-62767-0

[5] Davies, P. (2016) Environmental Degradation of Composites for Marine Structures: New Materials and New Applications. *Philosophical Transactions of the Royal Society*

A: Mathematical, Physical and Engineering Sciences, **374**, Article 20150272. https://doi.org/10.1098/rsta.2015.0272

[6] Aisyah, H.A., Paridah, M.T., Sapuan, S.M., Khalina, A., Berkalp, O.B., Lee, S.H., *et al*. (2019) Thermal Properties of Woven Kenaf/Carbon Fibre-Reinforced Epoxy Hybrid Composite Panels. *International Journal of Polymer Science*, **2019**, Article ID: 5258621. https://doi.org/10.1155/2019/5258621

[7] Azlin, M., Sapuan, S., Zuhri, M., Zainudin, E. and Ilyas, R. (2022) Thermal Stability, Dynamic Mechanical Analysis and Flammability Properties of Woven Kenaf/Polyester-Reinforced Polylactic Acid Hybrid Laminated Composites. *Polymers*, **14**, Article 2690. https://doi.org/10.3390/polym14132690

[8] Leonés, A., Peponi, L., García-Martínez, J. and Collar, E.P. (2022) Compositional Influence on the Morphology and Thermal Properties of Woven Non-Woven Mats of PLA/OLA/MgO Electrospun Fibers. *Polymers*, **14**, Article 2092. https://doi.org/10.3390/polym14102092

[9] Sofia, E. Putra, N. and Ali Gunawan, B. (2021) Evaluation of Indirect Evaporative Cooling Performance Integrated with Finned Heat Pipe and Luffa Cylindrica Fiber as Cooling/Wet Media. *Journal of Advanced Research in Experimental Fluid Mechanics and Heat Transfer*, **3**, 16-25.

[10] Qian, J., Li, Y., Xiang, Z., Cai, H. and Zhang, P. (2022) Effect of Weave Structure and Yarn Fineness on the Coolness and Thermal-Wet Comfort Properties of Woven Fabric. *Textile Research Journal*, **92**, 3782-3796. https://doi.org/10.1177/00405175221095891

[11] Singh, M., Dodla, S., Gautam, R.K. and Srivastava, V.K. (2022) Effect of Load, Sliding Frequency, and Temperature on Tribological Properties of Graphene Nanoplatelets Coated Carbon Fiber Reinforced Polymer Composites. *Journal of Composite Materials*, **57**, 121-132. https://doi.org/10.1177/00219983221140205

[12] Sabaghi, M., Taheri-Behrooz, F. and Salamat-Talab, M. (2022) Critical Strain Energy Release Rate of Woven Carbon/Epoxy Composites Subjected to Thermal Cyclic Loading. *Polymer Composites*, **43**, 6135-6149. https://doi.org/10.1002/pc.26919

[13] Njeugna, E., Tagne, N.R.S., Drean, J., Fokwa, D. and Harzallah, O. (2012) Mechanical Characterization of Raffia Fibres from *Raphia vinifera*. *International Journal of Mechanics Structural*, **3**, 1-17.

[14] Kendem Djoumessi, A., Sikame Tagne, R.N., Stanislas, T.T., Ngapgue, F. and Njeugna, E. (2022) Optimization of the Young's Modulus of Woven Composite Material Made by *Raphia Vinifiera* Fiber/Epoxy. *International Journal for Simulation and Multidisciplinary Design Optimization*, **13**, Article No. 21. https://doi.org/10.1051/smdo/2022014

[15] Sikame Tagne, N.R., Mbou, T.E., Harzallah, O., Ndapeu, D., Huisken, W., Nkemaja, D., *et al*. (2020) Physicochemical and Mechanical Characterization of *Raffia vinifera* Pith. *Advances in Materials Science and Engineering*, **2020**, Article ID: 8895913. https://doi.org/10.1155/2020/8895913

[16] Agrawal, S.A. (2021) Simplified Measurement of Density of Irregular Shaped Composites Material Using Archimedes Principle by Mixing Two Fluids Having Different Densities. *International Research Journal of Engineering and Technology*, **8**, 1005-1009.

[17] Damfeu, J.C., Meukam, P., Jannot, Y. and Wati, E. (2017) Modelling and Experimental Determination of Thermal Properties of Local Wet Building Materials. *Energy and Buildings*, **135**, 109-118. https://doi.org/10.1016/j.enbuild.2016.11.022

[18] Mbou Tiaya, E., Huisken Mejouyo, P.W., Ndema Ewane, P.A., Damfeu, C., Meukam,

P. and Njeugna, E. (2023) Effect of Particle Sizes on Physical, Thermal and Mechanical Behavior of a Hybrid Composite with Polymer Matrix with Raffia Vinifera Cork and Bambusa Vulgaris. *Polymer Bulletin*, **81**, 275-295. https://doi.org/10.1007/s00289-023-04702-y

[19] Lavanya, B. (2019) MHD Rotating Flow Through a Porous Medium with Heat and Mass Transfer. *Journal of Advanced Research in Fluid Mechanics and Thermal Sciences*, **54**, 221-231.

[20] Damfeu, J.C., Meukam, P. and Jannot, Y. (2016) Modeling and Estimation of the Thermal Properties of Clusters Aggregates for Construction Materials: The Case of Clusters Aggregates of Lateritic Soil, Sand and Pouzzolan. *International Journal of Heat and Mass Transfer*, **102**, 407-416. https://doi.org/10.1016/j.ijheatmasstransfer.2016.06.044

[21] Damfeu, J.C., Meukam, P. and Jannot, Y. (2016) Modeling and Measuring of the Thermal Properties of Insulating Vegetable Fibers by the Asymmetrical Hot Plate Method and the Radial Flux Method: Kapok, Coconut, Groundnut Shell Fiber and Rattan. *Thermochimica Acta*, **630**, 64-77. https://doi.org/10.1016/j.tca.2016.02.007

[22] Pycka, S. and Roman, K. (2023) Comparison of Wood-Based Biocomposites with Polylactic Acid (PLA) Density Profiles by Desaturation and X-Ray Spectrum Methods. *Materials*, **16**, Article 5729. https://doi.org/10.3390/ma16175729

[23] Audu, S., Aje, S., Isuwa, T. and Aji, S. (2019) Investigation of the Impact, Hardness, Density and Water Absorption of Polypropylene Filled Doum Palm Shell Particles Composite. *Journal of Information Engineering and Applications*, **9**, 28-37. https://doi.org/10.7176/jiea/8-1-04

[24] Sikame Tagne, N.R., Njeugna, E., Fogue, M., Drean, J.-Y., Nzeukou, A. and Fokwa, D. (2014) Study of Water Absorption in *Raffia vinifera* Fibres from Bandjoun, Cameroon. *The Scientific World Journal*, **2014**, Article ID: 912380. https://doi.org/10.1155/2014/912380

[25] Youbi, S.B.T., Harzallah, O., Tagne, N.R.S., Huisken, P.W.M., Stanislas, T.T., Drean, J., *et al*. (2023) Effect of *Raphia vinifera* Fibre Size and Reinforcement Ratio on the Physical and Mechanical Properties of an Epoxy Matrix Composite: Micromechanical Modelling and Weibull Analysis. *International Journal of Polymer Science*, **2023**, Article ID: 5591108. https://doi.org/10.1155/2023/5591108

[26] Kamaludin, N.H.I., Ismail, H., Rusli, A. and Ting, S.S. (2020) Thermal Behavior and Water Absorption Kinetics of Polylactic Acid/Chitosan Biocomposites. *Iranian Polymer Journal*, **30**, 135-147. https://doi.org/10.1007/s13726-020-00879-5

[27] Nsouandélé, J.L., Bonoma, B., Simo Tagne, M. and Njomo, D. (2010) Determination of the Diffusion Coefficient of Water in the Tropical Woods. *Physical and Chemical News*, **54**, 61-67.

[28] Liu, D., Xia, K., Yang, R., Li, J., Chen, K. and Nazhad, M. (2012) Manufacturing of a Biocomposite with Both Thermal and Acoustic Properties. *Journal of Composite Materials*, **46**, 1011-1020. https://doi.org/10.1177/0021998311414069

[29] Trigui, A., Karkri, M. and Boudaya, C. (2014) Propriétés thermophysiques et comportement thermique des composites avec ou sans changement de phase. *International Journal of Scientific Research & Engineering Technology*, **2**, 51-57.

[30] Osseni, S.O.G., Apovo, B.D. and Ahouannou, C. (2016) Caractérisation thermique des mortiers de ciment dopés en fibres de coco par la méthode du plan chaud asymétrique à une mesure de temperature. *Afrique Science*, **12**, 119-129.

[31] Ngono Mvondo, R.R., Lissouck, R.O., Bell, S. and Meukam, P. (2021) Investigation on Mechanical and Thermal Properties Related to Hygroscopicity of Two African

Hardwoods. *Wood Material Science & Engineering*, **17**, 846-857. https://doi.org/10.1080/17480272.2021.1967447

[32] Mvondo, R.R.N., Damfeu, J.C., Meukam, P. and Jannot, Y. (2019) Influence of Moisture Content on the Thermophysical Properties of Tropical Wood Species. *Heat and Mass Transfer*, **56**, 1365-1378. https://doi.org/10.1007/s00231-019-02795-8

[33] Castegnaro, S., Gomiero, C., Battisti, C., Poli, M., Basile, M., Barucco, P., *et al.* (2017) A Bio-Composite Racing Sailboat: Materials Selection, Design, Manufacturing and Sailing. *Ocean Engineering*, **133**, 142-150. https://doi.org/10.1016/j.oceaneng.2017.01.017

[34] Haramina, T., Hadžić, N. and Keran, Z. (2023) Epoxy Resin Biocomposites Reinforced with Flax and Hemp Fibers for Marine Applications. *Journal of Marine Science and Engineering*, **11**, Article 382. https://doi.org/10.3390/jmse11020382

[35] Sassane, N. Boubendira, K. Benfoughal, A. Boughedir, N. and Hamzaoui, N. (2017) Study of the Resilience of a Composite Material Intended for the Orthopedic Prosthesis of a Tibia. 23*ème Congrès Français de Mécanique*, Lille, 28 Août au 1er Septembre 2017, 1-11.

[36] De Almeida, O., Ferrero, J., Escalé, L. and Bernhart, G. (2018) Charpy Test Investigation of the Influence of Fabric Weave and Fibre Nature on Impact Properties of Peek-Reinforced Composites. *Journal of Thermoplastic Composite Materials*, **32**, 729-745. https://doi.org/10.1177/0892705718778744

[37] Defo, N., Sikame, R.N.T., Huisken, W.P.M., Ndapeu, D., Tido, S.T., Bistac-Brogly, S., *et al.* (2023) Development and Characterization of Agglomerated Abrasives Based on Agro-Industrial By-Products. *Journal of Natural Fibers*, **20**, Article 2178579. https://doi.org/10.1080/15440478.2023.2178579

[38] Aisyah, H.A., Paridah, M.T., Sapuan, S.M., Ilyas, R.A., Khalina, A., Nurazzi, N.M., *et al.* (2021) A Comprehensive Review on Advanced Sustainable Woven Natural Fibre Polymer Composites. *Polymers*, **13**, Article 471. https://doi.org/10.3390/polym13030471

[39] Zsidai, L. and Kátai, L. (2016) Abrasive Wear and Abrasion Testing of PA 6 and PEEK Composites in Small-Scale Model System. *Acta Polytechnica Hungarica*, **13**, 197-214. https://doi.org/10.12700/aph.13.6.2016.6.11

[40] Güneş, A., Düzcükoğlu, H., Salur, E., Aslan, A. and Şahin, Ö.S. (2023) Investigation of Friction Coefficient Changes in Recycled Composite Materials under Constant Load. *Lubricants*, **11**, Article 407. https://doi.org/10.3390/lubricants11090407

[41] Atakan, R., Sezer, S. and Karakas, H. (2018) Development of Nonwoven Automotive Carpets Made of Recycled PET Fibers with Improved Abrasion Resistance. *Journal of Industrial Textiles*, **49**, 835-857. https://doi.org/10.1177/1528083718798637

[42] Corradi, S., Isidori, T., Corradi, M., Soleri, F. and Olivari, L. (2009) Composite Boat Hulls with Bamboo Natural Fibres. *International Journal of Materials and Product Technology*, **36**, 73-89. https://doi.org/10.1504/ijmpt.2009.027821

[43] Basumatary, K.K., Mohanta, N. and Acharya, S.K. (2014) Effect of Fiber Loading on Abrasive Wear Behaviour of Ipomoea Carnea Reinforced Epoxy Composite. *International Journal of Plastics Technology*, **18**, 64-74. https://doi.org/10.1007/s12588-014-9065-0

[44] Patnaik, P.K., Swain, P.T.R. and Biswas, S. (2018) Investigation of Mechanical and Abrasive Wear Behavior of Blast Furnace Slag-Filled Needle-Punched Nonwoven Viscose Fabric Epoxy Hybrid Composites. *Polymer Composites*, **40**, 2335-2345. https://doi.org/10.1002/pc.25090

[45] Kaliappan, P., Kesavan, R. and Vijaya Ramnath, B. (2017) Investigation on Effect of

Fibre Hybridization and Orientation on Mechanical Behaviour of Natural Fibre Epoxy Composite. *Bulletin of Materials Science*, **40**, 773-782. https://doi.org/10.1007/s12034-017-1420-2

[46] Vijayakumar, S. and Palanikumar, K. (2019) Mechanical Property Evaluation of Hybrid Reinforced Epoxy Composite. *Materials Today: Proceedings*, **16**, 430-438. https://doi.org/10.1016/j.matpr.2019.05.111

[47] Vijaya Ramnath, B., Junaid Kokan, S., Niranjan Raja, R., Sathyanarayanan, R., Elanchezhian, C., Rajendra Prasad, A., *et al.* (2013) Evaluation of Mechanical Properties of Abaca-jute-glass Fibre Reinforced Epoxy Composite. *Materials & Design*, **51**, 357-366. https://doi.org/10.1016/j.matdes.2013.03.102